ACS OMEGA

http://pubs.acs.org/journal/acsodf

Article

# Solvent-Free Solid-State Lithium Battery Based on $LiFePO_4$ and MWCNT/PEO/PVDF-HFP for High-Temperature Applications

Han Yu, Ye Jin, Guodong David Zhan,* and Xinhua Liang*

Cite This: *ACS Omega* 2021, 6, 29060−29070

Read Online

ACCESS | Metrics & More | Article Recommendations | Supporting Information

**ABSTRACT:** Rechargeable lithium-ion batteries (LIBs) have a wide range of applications but face challenges in harsh working or operating environments at high temperatures. In this work, a solid polymer electrolyte with MWCNT-COOH as an additive (MWCNT-SPE) was obtained. MWCNT-SPE has a high thermal stability and can be used in high-temperature operating environments. Solid-state lithium batteries based on MWCNT-SPE and $LiFePO_4$ were assembled. The resulting lithium batteries exhibited excellent electrochemical properties at 70 and 120 °C, demonstrating a wide range of operations suitable for solid-state batteries with extreme demands. The symmetrical Li/MWCNT-SPE/Li cell operated for 1800 h with low polarization voltage and no short circuit, and the $LiFePO_4$/MWCNT-SPE/Li cell delivered superior cycling performance under both 0.2 and 0.5 C-rates, indicating that the interface compatibility between the lithium metal and MWCNT-SPE membrane was good and could effectively suppress the formation of lithium dendrites. The superior performance of the resulting MWCNT-SPE was due to the weak interaction between PEO, PVDF-HFP, and MWCNT-COOH, which reduced the tendency of PEO's crystallinity and thereby significantly increased the $Li^+$ migration ability and improved the cycling life of the batteries.

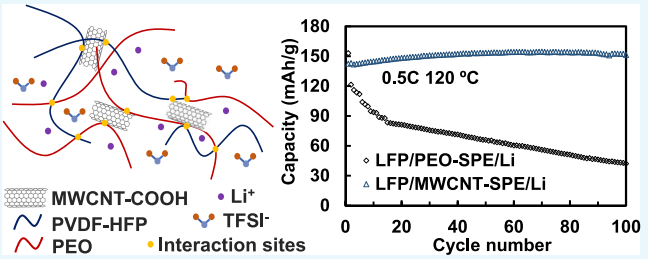


## 1. INTRODUCTION

Rechargeable lithium-ion batteries (LIBs) have been used in various aspects of life, but there is limitation for LIBs to be used in some high-temperature working environments due to the liquid electrolyte used in traditional LIBs. For example, batteries for handheld surgical tools need to be exposed to extreme temperatures, withstanding temperatures of up to 137 °C.[1] Measurement-while-drilling (MWD) tools in the petroleum drilling industry operate at temperatures of up to 150 °C.[2] Currently, batteries used in the high-temperature field are mainly primary batteries, such as Li-$SOCl_2$ primary batteries and NiMH batteries. The operating temperature of current commercial LIBs is −20 to 55 °C. Exceeding this temperature range will cause severe side reactions and increase the risk of thermal runaway. For example, the $LiPF_6$ salt in liquid electrolyte begins to decompose into HF above 55 °C, which will consume the active material, thereby reducing the battery performance. This problem will be much more serious at high temperatures.[3,4] Furthermore, the solid electrolyte interphase (SEI) is not stable when the operation temperature is over 65 °C; it will decompose and generate gas.[5−7] Therefore, modifying the electrolyte is the key to expand the operating temperature range of LIBs.

A solid-state electrolyte is considered to be a good solution to this issue, as the use of a solid electrolyte eliminates the need for a liquid electrolyte and simplifies battery design, thereby improving safety and durability.[8] Among all kind of solid-state electrolytes, inorganic solid electrolytes (ISEs) usually show high ionic conductivity comparable to that of liquid electrolytes, and some even exceed that of liquid electrolytes.[9] However, due to the brittleness and rigidity of ISEs, they normally have poor contact with adjacent electrodes without special treatment. This has dramatically hindered its applications.[10,11] In contrast, solid polymer electrolytes (SPEs) are mainly composed of a homogeneous mixture of solid polymers and lithium salts, which makes it possible to adjust the thickness arbitrarily and maintain flexible close contact with solid electrodes. Therefore, in terms of interface compatibility, SPEs are easier to meet the application needs of solid-state lithium metal batteries. After the first report of poly(ethylene oxide) (PEO)-alkali metal salt SPEs with ion doping, PEO-lithium salt composite electrolytes have been widely explored for lithium polymer batteries.[12−14] PEO-based SPEs are considered the most promising polymer matrix.[12,15,16] Due to the interaction between $Li^+$ and the ether oxygen atoms of the PEO matrix,[16] PEO is effective in solvating lithium salts, thereby providing the ability to transport lithium ions.[17] However, the test conditions for such batteries are generally

Received: August 9, 2021
Accepted: September 30, 2021
Published: October 19, 2021

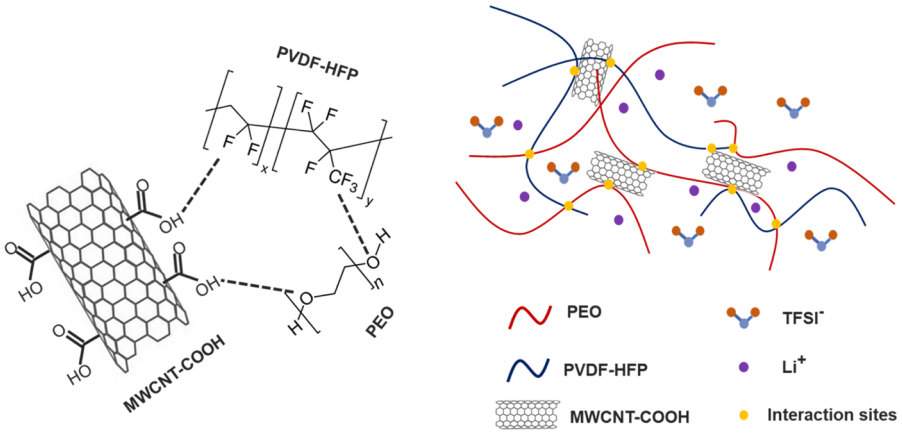


**Figure 1.** Molecular structures of PVDF-HFP, PEO, and MWCNT-COOH and schematic representation of a 3D polymer network of an SPE membrane formed by the intermolecular hydrogen bonding effects.

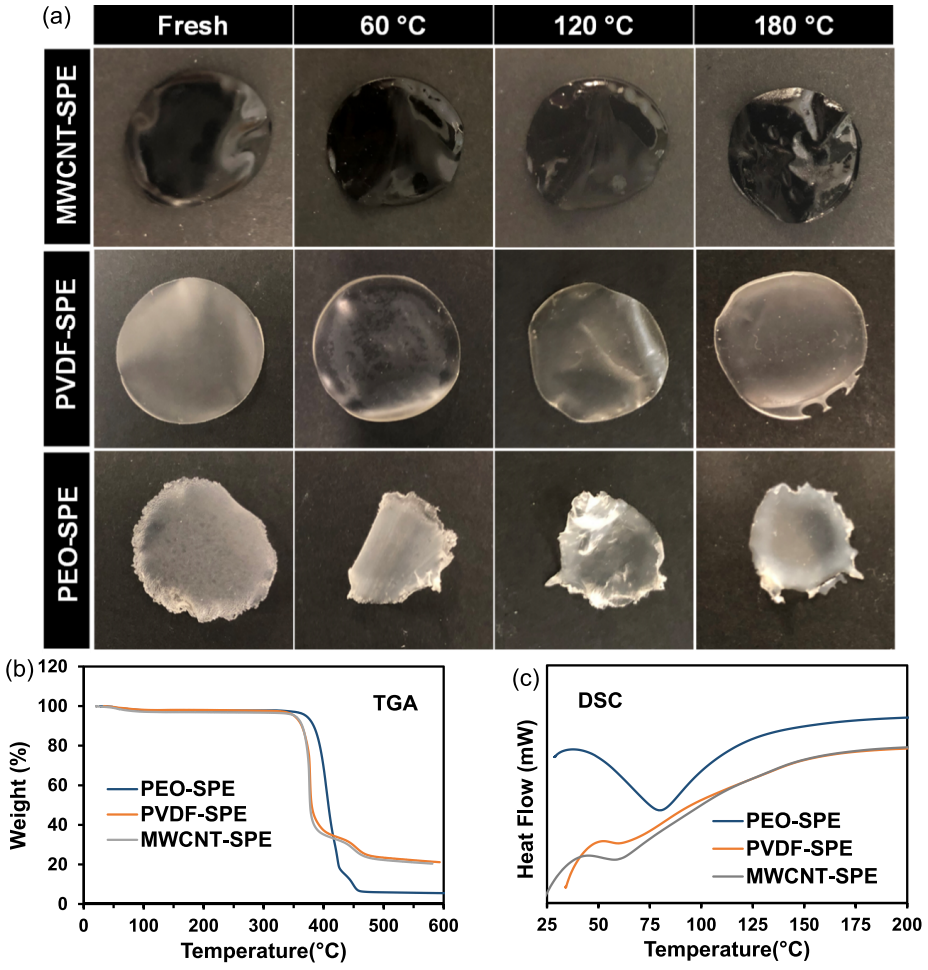


**Figure 2.** (a) Photos of as-prepared and annealed MWCNT-SPE, PVFD-SPE, and PEO-SPE membranes. Thermal stability of MWCNT-SPE, PVDF-SPE, and PEO-SPE membranes: (b) TGA curve and (c) DSC curve.

limited to 60 °C due to the limitation of the melting point of PEO. Such low temperatures cause very low ionic conductivity, leading to poor electrochemical performance; when the temperature is higher than 65 °C, the PEO membrane will melt and become unusable. Pure PEO-based SPE batteries tested above 65 °C have rarely been reported.

The addition of a filler to SPE is considered to be an effective strategy to address the problem of temperature limitation.[18] It was reported that a PI (polyimide) membrane filled with PEO and LiTFSI (bis(trifluoromethane)sulfonimide lithium salt) as a safe SPE could prevent short circuiting even after more than 1000 h of charge/discharge cycling.[19] It was found that the local $Li^+$ environments can be changed to activate more mobile $Li^+$ in the polymer by adding a filler material that has a strong interaction with the polymer electrolyte, thereby increasing the $Li^+$ conductivity of the


https://doi.org/10.1021/acsomega.1c04275
ACS Omega 2021, 6, 29060−29070

composite electrolyte.[20] PVDF-HFP (polyvinylidene fluoride-*co*-hexafluoropropylene) is frequently reported to be used as the matrix of a porous polymer electrolyte because it has higher ionic conductivity and lower crystallinity than other polymers.[21] However, it is still necessary to add a liquid electrolyte when this type of polymer electrolyte is used,[22,23] which still fails to avoid the problem of temperature limitation caused by the liquid electrolyte.

In this study, solvent-free LIBs were assembled based on MWCNT/PVDF-HFP/PEO based SPE. PVDF-HFP was used as the main matrix. PEO acted as a $Li^+$ conductor and formed diffusion channels in the matrix. LiTFSI provided Li ions. To better promote the mixing of PVDF-HFP and PEO and enhance the interaction between components, MWCNT-COOH was added as a binder. Through simple physical mixing, a solid electrolyte membrane with excellent thermal performance and ultra-high cycling stability was obtained. $LiFePO_4$ (LFP) is a very stable cathode material with a very flat voltage plateau at around 3.5 V, high theoretical specific capacity of about 170 mAh/g, and high thermal stability. Solid-state Li metal batteries based on LFP and SPE were assembled. The obtained batteries delivered excellent cycling stability at 120 °C.

## 2. RESULTS AND DISCUSSION

### 2.1. Characterizations of the Electrolyte Membrane.

To obtain a solid-state battery that can work stably and safely at high temperatures, a solid electrolyte membrane with sufficient thermal stability is the key. PEO has high crystallinity and low melting point, making it difficult to prepare large-area membranes. On the other hand, the obtained membranes are anisotropic, which is not conducive to the transmission of $Li^+$. By dispersing PEO in PVDF-HFP with a lower crystallinity, the crystallinity of PEO can be effectively reduced, and the membrane-forming properties of the prepared membrane can also be greatly improved. We tried different ratios of PVDF-HFP and PEO. The high content of PVDF-HFP makes it easier to get a thick and easy-to-form membrane, but at the same time, it results in poor ionic conductivity. If the loading of PEO is too high, the membrane-forming ability is poor, and the formed membrane is fragile. Due to the above-mentioned trade-off, we chose a mass ratio of PVD-HFP/PEO of 1:1 to obtain an ion-conducting and flexible membrane.

Figure 1 shows the molecular structure of PVDF-HFP, PEO, and MWCNT-COOH and the schematic representation of its film formation. Compared with other polymers, PVDF-HFP as the matrix of the SPE film has relatively low crystallinity, high ionic conductivity, and good mechanical stability.[24] PEO, as a $Li^+$ conductor, was blended with PVDF-HFP to form an SPE membrane. Meanwhile, the interaction of PVDF-HFP and PEO can effectively reduce the crystallinity of PEO, which is more conducive to the transmission of lithium ions.[25] According to a previous report, a small amount of additives with specific functional groups, such as the −COOH group, can promote the interaction between molecules, which can effectively improve the mechanical properties and thermal stability of the polymer.[26] In this study, functionalized MWCNT (MWCNT-COOH), containing a lot of −COOH groups, was used as the additive. In addition, according to the chemical structures of PVDF-HFP, PEO, and MWCNT-COOH, these molecules can form effective H−F bonds and H−O bonds with each other,[23,27] which can make the polymer chains more disorderly in the blending, further reducing the crystallinity of PEO and thus improving the ionic conductivity. In this paper, the SPE membrane with MWCNT-COOH as the additive was named MWCNT-SPE. For comparison, polymer electrolytes based on pure PEO and the blend of PVDF-HFP and PEO were also prepared and named PEO-SPE and PVDF-SPE, respectively.

As shown in Figure 2a, compared to the rough PEO-SPE membrane, it is easy to obtain a solid electrolyte membrane with a smooth surface with the addition of PVDF-HFP. Furthermore, the membrane obtained after adding MWCNT-COOH was more flexible and tougher. The thermal stability of the electrolyte is a key feature to determine whether an LIB is suitable for high-temperature environments or not. The mixed PEO/PVDF-HFP can increase the melting point of the forming membrane. Figure 2a shows all three SPE membranes after annealing from 60 to 180 °C (kept at 60, 120, and 180 °C for 2 h each). Both MWCNT-SPE and PVDF-SPE membranes showed almost no obvious shrinkage even after annealing at 180 °C for 2 h, which could be due to the high melting point of PVDF-HFP, as well as the strong interaction between PVDF-HFP and PEO. The addition of MWCNT-COOH can increase the number of interaction sites between polymer chains, thereby further enhancing this effect. The results of thermal stability indicate that the synthesized MWCNT-SPE would be able to survive in a high-temperature working environment.

The thermal stability of SPE membranes was analyzed by thermogravimetric analysis (TGA) and differential scanning calorimetry (DSC). As presented in TGA curves (Figure 2b), the MWCNT-SPE and PVDF-SPE membranes showed a thermal decomposition temperature of ∼375 °C, slightly lower than that of the PEO-SPE membrane, which was due to the lower decomposition temperature of PVDF-HFP. However, such decomposition temperature is still high enough for some high-temperature applications. Figure 2c shows DSC curves of all three SPE membranes. For the PEO-SPE membrane, a broad endothermic peak between 50 and 100 °C was assigned to the melting of PEO. Compared with the PEO membrane, both the PVDF-SPE and MWCNT-SPE membranes showed a small melting peak of PEO, and the melting point of PVDF-HFP was about 177 °C. However, from the DSC curve, no obvious endothermic peak belonging to PVDF-HFP was observed, indicating that PVDF-HFP inhibited the crystallization of PEO and PVDF-HFP.[28]

The scanning electron microscopy (SEM) images of PEO-SPE, PVDF-SPE, and MWCNT-SPE membranes are shown in Figure 3. The PEO membrane presented a smooth surface with some holes, but there were many cracks on the surface, as shown in Figure 3a,b. These cracks may be caused by the crystallization of PEO during the membrane formation process. When PVDF-HFP was added, the crystallization of PEO was inhibited. Therefore, the resulted PVDF-SPE showed a different surface morphology; unlike PEO-SPE, there were many radial lines on the surface of PVDF-SPE (Figure 3c,d). This could be due to the interaction of PVDF-HFP and PEO, which caused the crystalline morphology of PEO to change.[29] There were still some holes on the surface of the PVDF-SPE membrane, but there were no cracks. After adding MWCNT-COOH, the membrane surface became smoother. There were no holes or cracks on the surface of the membrane (Figure 3e,f). This indicated that the additive promoted the formation of amorphous polymer films, which might lead to the enhancement of the segmented movement of polymer chains.


https://doi.org/10.1021/acsomega.1c04275
ACS Omega 2021, 6, 29060−29070

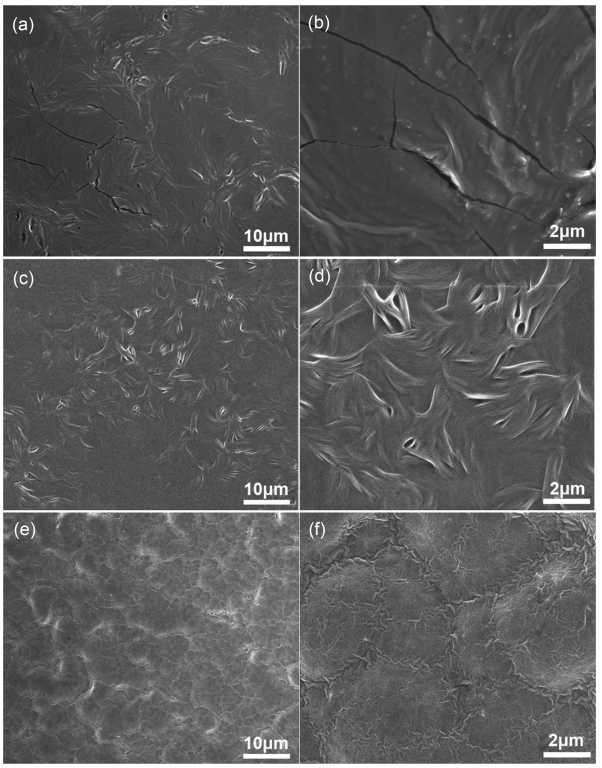


**Figure 3.** SEM images of the surface of (a, b) PEO-SPE, (c, d) PVDF-SPE, and (e, f) MWCNT-SPE membranes.

Furthermore, compared to membranes containing crystalline regions, the amorphous membrane also demonstrates better interface compatibility with lithium metal anode and cathode electrodes.

To investigate the influences of interaction between MWCNT-COOH, PVDF-HFP, and PEO and the interaction between PEO and LiTFSI on the crystallinity of the membrane, X-ray diffraction (XRD) was conducted on pure PEO, PVDF-HFP, LiTFSI, and different SPE membranes. As shown in Figure 4, both XRD patterns of PEO and LiTSFI had visible characteristic peaks, and the characteristic peak intensity of PEO was very high. When LiTFSI was dissolved into PEO, all the characteristic peaks of LiTFSI in the resulting electrolyte membrane disappeared, indicating that LiTFSI was well dispersed in PEO. Notably, there was almost no change in the position and intensity of PEO crystalline peaks compared to those of pure PEO, indicating that PEO still existed mainly as a crystalline in PEO-SPE membranes.

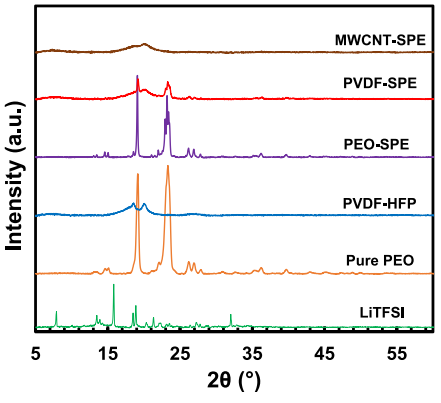


**Figure 4.** XRD patterns of pure LiTFSI, pure PEO, pure PVDF-HFP, the PEO-SPE membrane, the PVDF-SPE membrane, and the MWCNT-SPE membrane.

When PVDF-HFP was mixed with PEO and LiTFSI, the crystal peaks of PEO and LiTFSI overlapped with the low-intensity peaks of the PVDF-HFP semicrystalline phase. However, characteristic peaks belonging to PEO could still be observed, indicating that the interaction between PEO and PVDF-HFP can destroy the crystallization of PEO and reduce the crystallinity of the prepared electrolyte membrane to some extent. When MWCNT-COOH was added, the crystal peak of PEO between 25 and 45° almost disappeared, and the peak belonging to PVDF-HFP left only a very broad peak, which indicates that the addition of MWCNT-COOH effectively promoted the interaction between molecules, reduced the crystalline phase, increased the amorphous area, and formed a more disordered polymer membrane.

With the addition of lithium salt into the polymer matrix, it is expected that the cations of the salt will coordinate with polar groups in the host polymer matrix, resulting in complexation. In addition, there are weak interactions between polymer chains and the additive. These types of interactions will influence the local structure of the polymer backbone, and certain infrared active modes of vibration will be affected. To understand the interactions between lithium salt and the polymer hosts in the polymer electrolytes, Fourier transform infrared (FT-IR) transmission spectra of the complexes were collected at room temperature in a region of 4000−400 $cm^{-1}$. The full spectrum with peak positions is shown in Figure S1. Figure 5 shows the FTIR spectra of pure PEO, PVDF-HFP, LiTFSI, PEO-SPE, PVDF-SPE, and MWCNT-SPE.

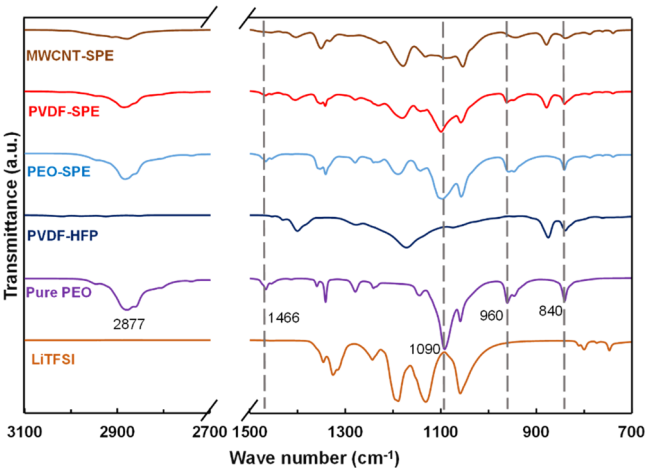


**Figure 5.** FTIR spectra of pure PEO, pure PVDF-HFP, pure LiTFSI, the PEO-SPE membrane, the PVDF-SPE membrane, and the MWCNT-SPE membrane.

In the spectrum of pure PEO, a broad band at 2877 $cm^{-1}$ is ascribed to the −CH symmetric stretching of PEO, a band at 1466 $cm^{-1}$ represents the asymmetric bending of C−H in PEO, and the characteristic vibrational band at 1090 $cm^{-1}$ belongs to the stretching of C−O−C in PEO. The bands around 960 and 840 $cm^{-1}$ are $-CH_2$ twisting and $-CH_2$ wagging, respectively, which are characteristic peaks of PEO.[30] PVDF-HFP contains free electron pairs at the fluorine (F) atoms of $-CF_2$ and $-CF_3$ groups. The characteristic bands of $-CH_2$ wagging and antisymmetric $-CF_2$ stretching are at 1399


https://doi.org/10.1021/acsomega.1c04275
ACS Omega 2021, 6, 29060−29070

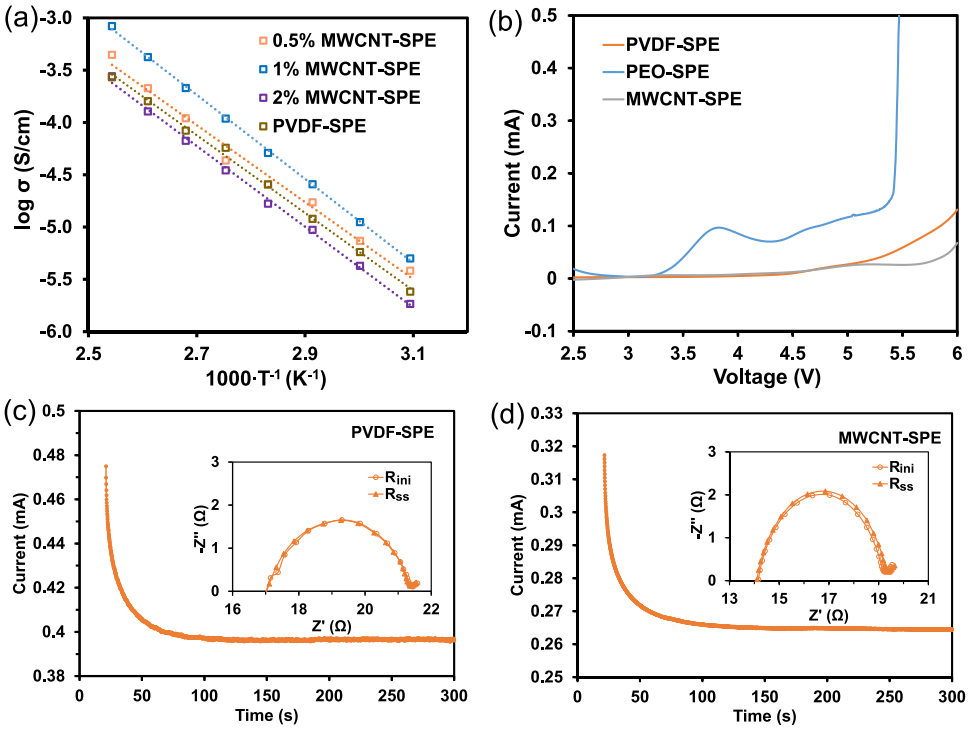


**Figure 6.** (a) Arrhenius plots of ionic conductivity versus temperature for SPE membranes. (b) Linear sweep voltammograms of PEO-SPE, PVDF-SPE, and MWCNT-SPE at 120 °C. DC polarization curves of the (c) Li/PVDF-SPE/Li symmetric cell and (d) Li/MWCNT-SPE/Li symmetric cell at 120 °C.

and 1169 $cm^{-1}$, respectively, and the band at 875 $cm^{-1}$ is assigned to the vinylidene group of PVDF-HFP.[31] In the spectrum of pure LiTFSI, the characteristic bands at 1058, 1130, and 1190 $cm^{-1}$ are assigned to the asymmetric stretching of S−N−S, S═O bonding, and C−$SO_2$−N bonding, respectively.[32]

The most direct evidence that confirms the complexation of the polymer host with the lithium salt is the change in the strength and the shifting of the bands. In the spectrum of all three SPE membranes, all characteristic bands could be observed. Compared to pure LiTFSI, in all three SPE membranes, the characteristic peaks of LiTFSI were broadened or even disappeared. This was due to the low content of LiTFSI, and it was uniformly dispersed in the polymer matrix. The anions of LiTFSI coordinated with the ether carbon groups present in the polymers.[33] In PEO-SPE, all characteristic peaks of PEO could be observed. However, after blending with PVDF-HFP, the characteristic peaks of PEO became weaker and broader, such as peaks at 960, 1090, and 1466 $cm^{-1}$. This was due to the interaction between the −F group in PVDF-HFP and the C−O−C group, and the −OH group in PEO.[34] This change was more obvious when MWCNT-COOH was added. The characteristic peaks of PEO almost disappeared. This was attributed to the specific interaction between −COOH groups in MWCNT-COOH, −F groups in PVDF, and C−O−C groups in PEO. All of these changes confirmed the complexation and interaction between PEO, PVDF-HFP, and MWCNT-COOH. The interaction between MWCNT-COOH, PEO, and PVDF-HFP further promoted the dispersion of PEO in the polymer matrix.

**2.2. Electrochemical Performance.** As mentioned above, the introduction of polymer fillers and additive can reduce the crystallinity of PEO and promote the segment movement of PEO so that the ionic conductivity of the SPE membrane can be improved. To obtain an optimum loading of MWCNT-COOH, MWCNT-SPE membranes with different ratios of MWCNT-COOH were prepared, and the ionic conductivity of these films was measured. The Nyquist plots of all Li/SPE/Li cells at different temperatures are shown in Figure S2. The ionic conductivities of SPE were calculated based on the Nyquist plots using the equation $\sigma = \frac{d}{A \cdot R}$, where $d$ stands for the thickness of the solid-state electrolyte membrane (cm), $A$ stands for the projected area of the lithium electrode ($cm^2$), and $R$ stands for the impedance calculated from the Nyquist plot (Ω). The results are shown in Figure 6a. Compared with the SPE membrane without MWCNT-COOH, the ionic conductivity of the membrane slightly increased by adding 0.5 wt % of MWCNT-COOH. When the content reached 1 wt %, the highest ion conductivity was obtained. With 2 wt % of MWCNT-COOH, the ionic conductivity was lower than that of the one without additive. Therefore, for battery assembly in the following studies, 1 wt % MWCNT-SPE was used as the solid electrolyte.

The activation energy ($E_a$) values of SPEs can be extracted from the plots using the Arrhenius equation. The activation energy of the melting zone was much smaller than that of the solid zone, indicating that the melting of PEO at high temperature enhanced the $Li^+$ transfer kinetics.[35] Moreover, the interaction between MWCNT-COOH, the PEO polymer, and the PVDF-HFP polymer matrix can reduce the crystallinity of PEO and enhance the segment movement of the polymer backbone, thereby promoting lithium ion migration.[36] The $E_a$ values for SPE and MWCNT-SPE were 0.78 and 0.79 eV, respectively. Compared with the liquid electrolyte case with perfect contact between the liquid electrolyte and electrode sheet, the contact resistance and activation energy between the solid electrolyte and the electrode sheet were slightly larger.


https://doi.org/10.1021/acsomega.1c04275
ACS Omega 2021, 6, 29060−29070

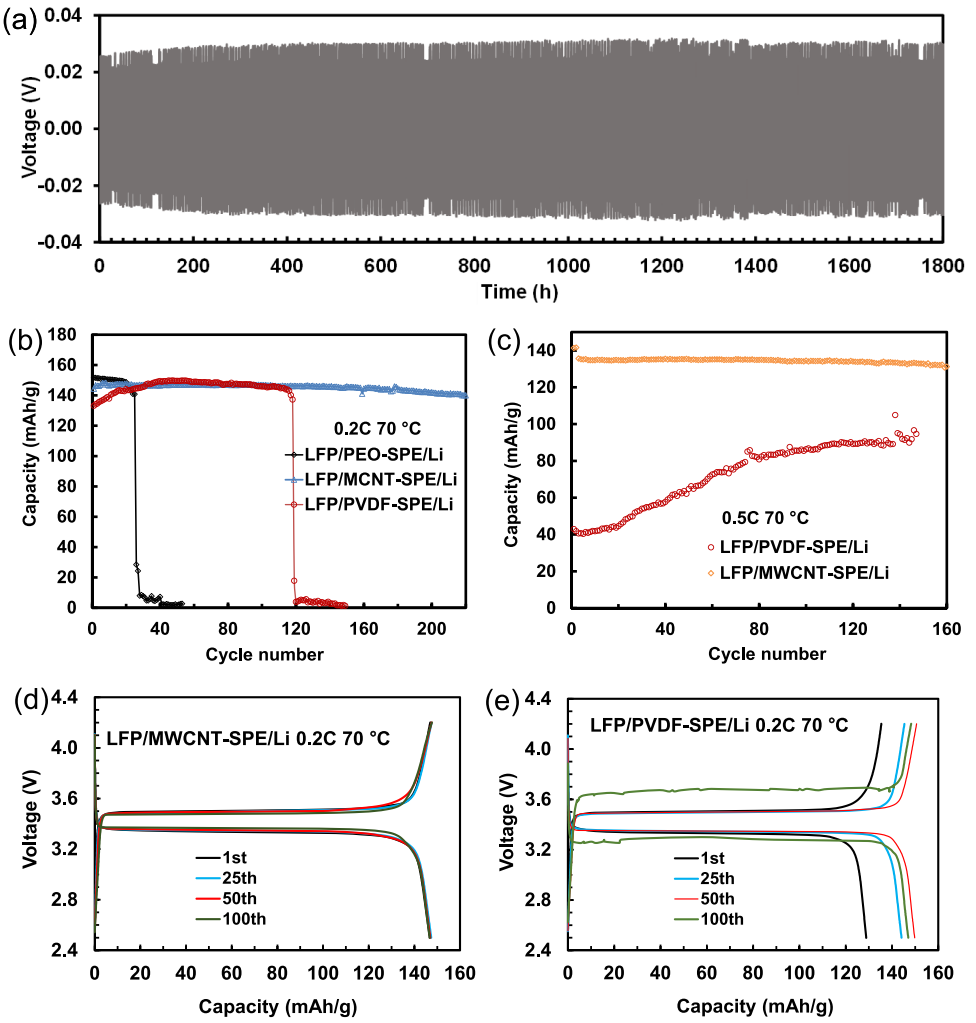


**Figure 7.** (a) Galvanostatic cycling curve of the Li/MWCNT-SPE/Li symmetric cell at 0.05 mA/cm$^2$. Cycling performance of all $LiFePO_4$/SPE/Li cells at (b) 0.2 C-rate and (c) 0.5 C-rate at 70 °C. The 1st, 25th, 50th, and 100th voltage capacity profiles of the (d) $LiFePO_4$/MWCNT-PEO/Li cell and (e) $LiFePO_4$/PVDF-SPE/Li cell.

In addition to the inherent ionic conductivity of the solid polymer electrolyte, the electrochemical stability of the solid polymer electrolyte and the value of lithium-ion transference numbers ($t_{Li+}$) are also important factors to be considered. To investigate the electrochemical stability of the prepared SPE membranes, Li/SPE/stainless-steel cells were assembled, and linear sweep voltammogram (LSV) tests were conducted in a potential range of 0−6.0 V *vs* Li/Li$^+$ with a scan rate of 1 mV/s at 120 °C, as shown in Figure 6b. These was no noticeable increase in the anodic current below 5.2 V for both PVDF-SPE and MWCNT-SPE membranes. However, the PEO-SPE membrane only exhibited a stable electrochemical window below 3.5 V. The good electrochemical stability of PVDF-SPE and MWCNT-SPE could be attributed to the PVDF-HFP matrix, as it can remove impurities at the interface, thereby reducing the occurrence of side reactions between impurities and the lithium metal electrode.[37]

During the charge/discharge process, a lithium-ion concentration gradient will form at the interface between the lithium metal electrode and electrolyte, which will result in an uneven distribution of lithium ions and the formation of lithium dendrites. The value of $t_{Li+}$ can be used to predict the degree of inhibition of lithium dendrites.[38] The larger the value of $t_{Li+}$ is, the better is the inhibition of the formation of dendritic lithium between the interface of the lithium metal and electrolyte.[39] In this study, the $t_{Li+}$ values of all three SPE membranes were calculated via direct current (DC) polarization and impedance measurements. The Nyquist plots of Li symmetric cells with PVDF-SPE and MWCNT-SPE membranes before and after polarization at 10 mV and 120 °C were collected, as shown in Figure 6,dc,d. The $t_{Li+}$ values in the case of Li/PVDF-SPE/Li and Li/MWCNT-SPE/Li were 0.82 and 0.84 at 120 °C, respectively. Compared to that of PVDF-SPE, the increased $t_{Li+}$ value of MWCNT-SPE can be attributed to the Li$^+$ transmission channel provided by the interaction of PVDF-HFP and PEO. We also compared the polarization curves of PEO-SPE, PVDF-SPE, and MWCNT-SPE at 70 °C, as shown in Figure S3. The lithium-ion transference numbers in the case of Li/PVDF-SPE/Li and Li/MWCNT-SPE/Li were 0.42 and 0.69, respectively. However, the $t_{Li+}$ value of PEO-SPE was only 0.19. The large $t_{Li+}$ value of MWCNT-SPE, compared to that of PVDF-SPE and PEO-SPE, foreshadowed a better performance in preventing the formation of lithium dendrites. In addition, compared to the results in Figure 6,dc,d, the stabilization time required for SPE at 120 °C was much shorter than that at 70 °C. This indicates that this type of solid-state battery was more conducive in a higher-temperature working environment.



https://doi.org/10.1021/acsomega.1c04275
ACS Omega 2021, 6, 29060−29070

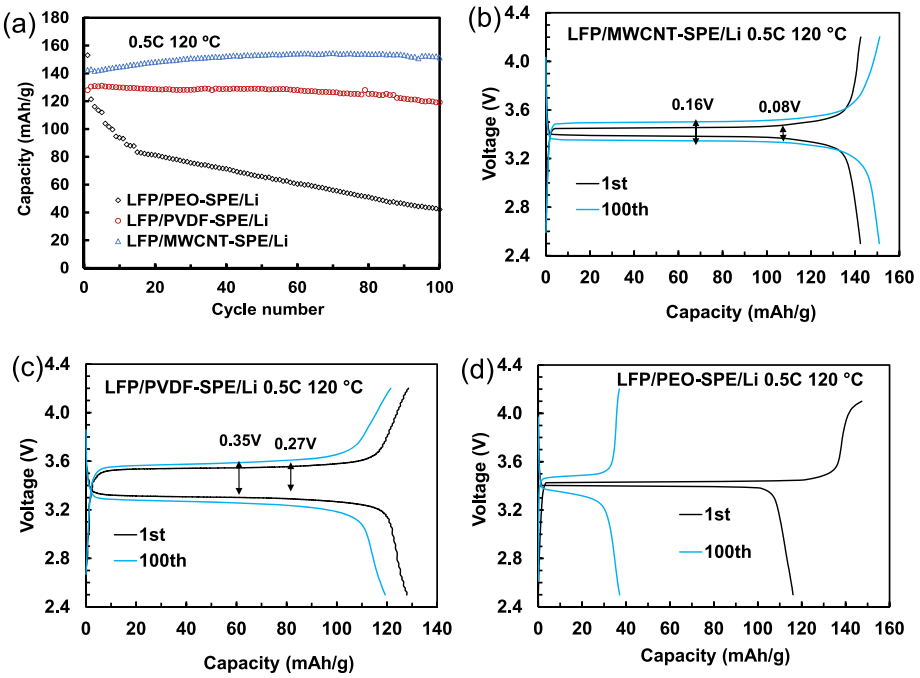


**Figure 8.** (a) Cycling performance of $LiFePO_4$/MWCNT-SPE/Li, $LiFePO_4$/PVDF-SPE/Li, and $LiFePO_4$/PEO-SPE/Li cells at 120 °C and a 0.5 C-rate and (b, c, d) the 1st and 100th voltage *vs* capacity profits of the (b) $LiFePO_4$/MWCNT-SPE/Li cell, (c) $LiFePO_4$/PVDF-SPE/Li cell, and (d) $LiFePO_4$/PEO-SPE/Li cell.

To evaluate the compatibility of different SPE membranes and lithium metal and the long-term mechanical stability of SPE membranes against the formation of Li dendrites, the symmetric Li/Li cells were cycled at a current density of 0.05 $mA/cm^2$ at 70 °C. The MWCNT-SPE based lithium symmetric cell delivered a low and steady potential of about ±0.03 V for over 1800 h of charge/discharge cycling, and no short circuit appeared, indicating the successful inhibition of dendritic lithium formation. In contrast, the voltage of the PEO-SPE based lithium symmetric cell dropped sharply after only 100 h of charge/discharge cycling, indicating that an internal short circuit was caused by the formation of excessive Li dendrites, as shown in Figure S4. PVDF-SPE based lithium symmetrical batteries also provided a low and stable potential for more than 1300 h, but after that, the same short circuit occurred.

The obtained MWCNT-SPE membrane can withstand temperatures over 180 °C without noticeable shrinkage (Figure 2). To test the charge/discharge cycling performance, a wide temperature window (from 70 to 120 °C) was applied for the assembled coin cells. Figure 7b shows the discharging performance of all $LiFePO_4$/SPE/Li cells at a 0.2 C-rate. The PEO-SPE based lithium battery delivered the highest initial discharge capacity (about 152 mAh/g). However, after 25 cycles of charge/discharge, the battery was short circuited due to the formation of lithium dendrites. In contrast, an excellent discharge performance of the $LiFePO_4$/MWCNT-SPE/Li cell was achieved at 70 °C, the MWCNT-SPE based battery showed a stable cycling performance, and its discharge capacity at the 220th cycle was about 142 mAh/g with a capacity retention of over 95%. For the PVDF-SPE based battery, a short circuit also appeared after 110 cycles of charge/discharge, the initial discharge capacity was 134 mAh/g, and the discharge capacity gradually increased in the subsequent cycling process. This could be due to the lack of compatibility between the electrolyte and the electrode sheet, as the crystalline regions still existed in the PVDF-SPE membrane. This phenomenon was more obvious in the charge/discharge at a 0.5 C-rate, as shown in Figure 7c. The PVDF-SPE based lithium battery only exhibited an initial discharge capacity of 40 mAh/g at a 0.5 C-rate, while the discharge capacity of MWCNT-SPE was 136 mAh/g, and the cycle stability was the same as the case at a 0.2 C-rate. These results confirmed the good compatibility of the synthesized MWCNT-SPE electrolyte with the metallic lithium and $LiFePO_4$ electrode.

Figure 7d,e shows the 1st, 25th, 50th, and 100th voltage capacity profiles of the $LiFePO_4$/MWCNT-SPE/Li cell and $LiFePO_4$/PVDF-SPE/Li cell. The MWCNT-SPE based battery showed a very stable charge/discharge platform within 100 cycles. However, for the PVDF-SPE based battery, the polarization voltage increased significantly after 100 cycles of charge/discharge. Some irregular waves appeared on the charge/discharge curve. This phenomenon also appeared on the voltage-capacity profiles of the PEO-SPE based battery after 25 cycles of charge/discharge (shown in Figure S5), which was caused by the formation of lithium dendrites. Further growth of dendritic lithium could pierce the electrolyte, resulting in a battery short circuit, and the performance of the battery could immediately be reduced to a minimum.

The electrochemical performance of all three different SPE based lithium batteries cycling at 120 °C is shown in Figure 8. Even at such a high temperature, the MWCNT-SPE based battery delivered a stable discharge performance, which was much better than that of PEO-SPE. As shown in Figure 8a, the initial discharge capacity of the MWCNT-SPE based lithium battery reached 142 mAh/g and still retained 152 mAh/g after 100 cycles of charge/discharge. The SPE-based lithium batteries also performed well. Compared to the case cycling at 70 °C, the PVDF-SPE based battery did not show any


https://doi.org/10.1021/acsomega.1c04275
ACS Omega 2021, 6, 29060−29070

obvious interface compatibility problem at 120 °C, which could be the result of the PVDF-SPE membrane that was fully softened at 120 °C. The C-rate performance exhibited similar results, as shown in Figure S6. Both PVDF-SPE and MWCNT-SPE based batteries delivered similar discharge capacity at a low C-rate; however, when the C-rate increased to 0.4C, the difference between PVDF-SPE and MWCNT-SPE increased, and the stability of MWCNT-SPE was better than that of PVDF-SPE. In contrast, the $LiFePO_4$/PEO-SPE/Li battery could not maintain effective charge/discharge cycling, the discharge capacity kept decreasing since the first cycle, and the capacity retention was only 64% after 15 cycles of charge/discharge. Figure 8b–d shows the 1st and 100th voltage capacity profiles of all three $LiFePO_4$/SPE/Li cells. The $LiFePO_4$/MWCNT-SPE/Li cell exhibited a pair of long charge/discharge voltage plateaus with a small gap (0.08 and 0.16 V at the 1st and 100th cycle, respectively). Although the SPE based battery could also cycle stably, its polarization voltage was significantly larger, which indicates that the interface compatibility between the MWCNT-SPE membrane and electrodes at high temperature was still much better than that of the PVDF-SPE membrane. The $LiFePO_4$/PEO-SPE/Li cell exhibited an excellent charge/discharge curve for the first cycle, and an extremely small voltage gap could be caused by the thinning of the electrolyte membrane due to the melting of PEO at high temperature, which made the contact distance between the electrodes closer. However, a low Coulombic efficiency in the first cycle indicated that a large amount of SEI was formed during the first cycle. This phenomenon also led to the rapid degradation of PEO-SPE based battery performance.

**2.3. Characterizations of Cycled SPE Membranes.** To reveal the mechanisms for the enhanced performance of the MWCNT-SPE based coin cells, FTIR was performed to characterize the solid electrolyte membrane after cycling. To exclude the influence of high-temperature heating, we also characterized all different SPE membranes after annealing at 120 °C, as shown in Figure 9. There was no obvious difference in the FTIR spectra between fresh electrolyte membranes and the electrolyte membranes after annealing at 120 °C. However, after 100 cycles of charge/discharge, some new peaks were observed on the PEO-SPE membrane. The strong bonds at 1632 and 839 $cm^{-1}$ indicated the formation of SEI due to the decomposition of PEO during cycling,[40−42] and the formation of SEI consumed the PEO and Li-salt, which resulted in the rapid performance reduction of pure PEO-SPE based coin cells. It is well known that the formation of SEI does not inhibit the formation of lithium dendrites.[43] Therefore, after reciprocating cycles, the performance curve of the PEO coin cells at 120 °C looked smoother than that at 70 °C. This could be due to the rapid decrease in electrochemical performance, which reduced the intercalation/deintercalation of $Li^+$ during a cycling process and, thereby, reduced the formation of lithium dendrites. Compared to the PEO-SPE membrane, the FTIR spectrum of the cycled MWCNT-SPE membrane only showed a small new weak peak at 1632 $cm^{-1}$, indicating that the MWCNT-SPE membrane effectively inhibited the decomposition of PEO and the formation of SEI. This is consistent with the improved electrochemical stability of MWCNT-SPE obtained in LSV.

## 3. CONCLUSIONS

A solid polymer electrolyte was prepared by complexing MWCNT-COOH, PEO, PVDF-HFP, and LiTFSI. The flexible

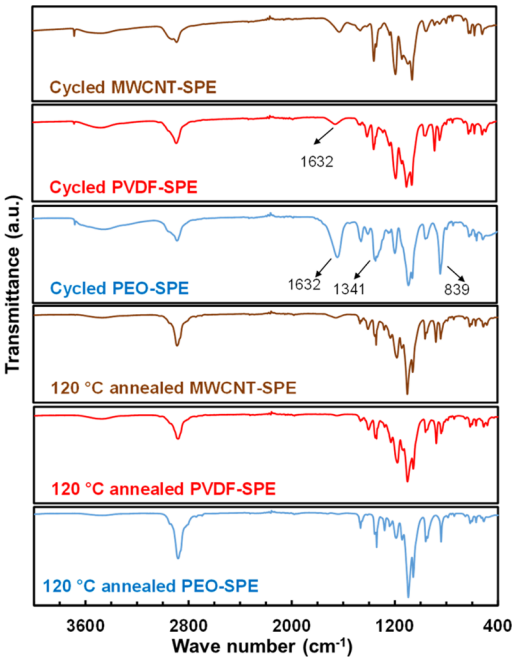


**Figure 9.** FTIR spectra of three SPE membranes annealed at 120 °C and cycled PEO-SPE, PVDF-SPE, and MWCNT-SPE membranes.

MWCNT-SPE membrane presented a high thermal stability up to 400 °C, and there was no obvious shrinkage after annealing at 180 °C. Solid-state lithium batteries based on the obtained SPE membranes and $LiFePO_4$ were assembled. The tailored MWCNT-SPE possessed a wide working temperature window based on electrochemical measurements from 70 to 120 °C, suitable for solid-state batteries with high-temperature working environments. The symmetric Li/MWCNT-SPE/Li cell ran at 70 °C for 1800 h and demonstrated low polarization voltage without any short circuit, which indicates that there was good interface compatibility between the Li anode and MWCNT-SPE membrane, and MWCNT-SPE could well inhibit the formation of lithium dendrites. The assembled $LiFePO_4$/MWCNT-SPE/Li cell delivered a capacity of 150 mAh/g at a 0.5 C-rate at 120 °C (with respect to $LiFePO_4$) and had a capacity retention of nearly 100% after 100 cycles of charge/discharge. The superior performance of the resulting MWCNT-SPE was mainly due to the weak interaction between MWCNT-COOH, PEO, and PVDF-HFP, which reduced the crystallinity of PEO and thus improved the $Li^+$ migration ability. The thermally stable PVDF-HFP improved the heat resistance of the electrolyte, thereby increasing the operating temperature range. The improvement of electrochemical stability effectively prevented the decomposition of PEO and inhibited the formation of lithium dendrites. In summary, the MWCNT-SPE membrane can provide an effective solution for solid-state lithium metal batteries.

## 4. EXPERIMENTAL SECTION

**4.1. Electrolyte Preparation.** In a typical procedure, 3 mg of MWCNT-COOH (US Nano) and 300 mg of PVDF-HFP (Sigma Aldrich) were first dissolved in 10 mL of DMF (dimethylformamide) (Sigma Aldrich) at 60 °C, and then 300 mg of PEO (Sigma Aldrich, Mv of ~600,000) and 100 mg of LiTFSI (Sigma Aldrich) were added into the solution and stirred continuously for 1 h at 70 °C to form a gel-like solution. The gel-like solution was treated by sonication for 2 h. After


https://doi.org/10.1021/acsomega.1c04275
ACS Omega 2021, 6, 29060−29070

that, the resulted solution was dropped on a disk and heated at 55 °C for 5 h to evaporate DMF. The resulted SPE membrane was peeled off from the disk after cooling to room temperature. Then, the obtained membrane was vacuum dried overnight at 55 °C. Finally, the obtained electrolyte membrane was transferred to a glove box and used directly for coin cell assembly. The thickness of all SPE membranes was around 50 $\mu$m.

**4.2. Electrode Preparation and Coin Cell Assembly.** Twenty-five milligrams of PEO and 25 mg of PVDF-HFP were dissolved in 2 mL of *N*-methyl-2-pyrrolidone (NMP) at 60 °C and continuously stirred to form a viscous homogeneous solution. Twenty-five milligrams of LiTFSI, 50 mg of carbon black, and 0.2 g of LFP were added to the solution. After the slurry was fully mixed, it was cast uniformly on an aluminum foil and then dried to obtain cathode electrodes. The obtained electrode sheet was punched into disks with an area of 0.71 $cm^2$. The typical mass loading of the electrodes was about 4 $mg/cm^2$. CR2032-type coin cells were assembled in an argon-filled dry glove box. LFP was used as the cathode, the Li metal foil was used as the anode, and the SPE membrane was used as the electrolyte as well as the separator.

**4.3. Electrochemical Testing.** A potentiostat (Biologic) was used to collect the electrochemical information. Li/Li symmetric batteries with all three different SPEs as electrolyte were assembled separately. The electrochemical impedance spectroscopy (EIS) of the Li/Li symmetric batteries in the temperature range of 40 to 120 °C was collected, with a frequency range from 1 Hz to 1 MHz, and the corresponding ionic conductivity of all three SPEs was calculated according to the following equation:

$$\sigma = \frac{d}{A \cdot R} \tag{1}$$

The electrochemical stability of the SPEs was tested by cycling Li/Li symmetric batteries at a constant current density of 0.1 mA/cm using a Neware battery tester. The batteries were periodically cycled for 1 h per cycle (0.5 h of charging and 0.5 h of discharging).

The $t_{Li+}$ values of different SPE membranes were calculated via DC polarization and impedance measurements. The initial resistance ($R_{ini}$, Ω) was calculated from the EIS data in an initial state of the Li/Li symmetric cell. The EIS data were collected in a frequency range of 100 kHz to 1 Hz under open circuit conditions.[44] Then, a 10 mV polarization bias of $\Delta V$ (mV) was applied to the battery to obtain the initial current ($I_{ini}$, mA). After the steady state was reached, the steady-state current ($I_{ss}$, mA) and resistance ($R_{ss}$, Ω) could be obtained. Then, $t_{Li+}$ was calculated using the following equation:

$$t_{Li^+} = \frac{I_{ss}R_{ss}(\Delta V - I_{ini}R_{ini})}{I_{ini}R_{ini}(\Delta V - I_{ss}R_{ss})} \tag{2}$$

**4.4. Material Characterizations.** A Q600 SDT TA instrument was used to analyze the thermal stability of different SPE membranes under an argon atmosphere at a heating rate of 10 °C/min from room temperature to 800 °C. A Nicolet IS50 spectrometer was used to collect the FTIR spectra of SPE membranes. The activation energy ($E_a$) was used to evaluate the $Li^+$ transfer capability of SPE membranes, which involves $Li^+$ dissociation and migration. A small $E_a$ value implies a lower energy needed for $Li^+$ transfer through SPE membranes. $E_a$ can be extracted from the following equation:

$$\sigma = A\exp\left(-\frac{Ea}{k \cdot T}\right) \tag{3}$$

where $\sigma$, $A$, $k$, and $T$ are the ionic conductivity, pre-exponential factor, Boltzmann constant, and absolute temperature, respectively.

## ■ ASSOCIATED CONTENT

### Supporting Information

The Supporting Information is available free of charge at https://pubs.acs.org/doi/10.1021/acsomega.1c04275.

FTIR spectra of SPE membranes (Figure S1); Nyquist plots of Li/MWCNT-SPE/Li with different ratios of MWCNT-COOH (Figure S2); DC polarization curves of Li/Li symmetric cells (Figure S3); galvanostatic cycling curves of Li/SPE/Li and Li/PEO/Li symmetric cells (Figure S4); cycling performance of $LiFePO_4$/PEO/Li cells (Figure S5); and C-rate performance of $LiFePO_4$/MWCNT-SPE/Li and $LiFePO_4$/SPE/Li cells (Figure S6) (PDF)

## ■ AUTHOR INFORMATION


### Corresponding Authors

**Guodong David Zhan** − *Drilling Technology Division, Exploration and Petroleum Engineering Center-Advanced Research Center (EXPECARC), Saudi Aramco, Dhahran 31311, Saudi Arabia*; Email: guodong.zhan@aramco.com

**Xinhua Liang** − *Linda and Bipin Doshi Department of Chemical and Biochemical Engineering, Missouri University of Science and Technology, Rolla, Missouri 65409, United States*; orcid.org/0000-0001-7979-0532; Email: liangxin@mst.edu

### Authors

**Han Yu** − *Linda and Bipin Doshi Department of Chemical and Biochemical Engineering, Missouri University of Science and Technology, Rolla, Missouri 65409, United States*

**Ye Jin** − *Linda and Bipin Doshi Department of Chemical and Biochemical Engineering, Missouri University of Science and Technology, Rolla, Missouri 65409, United States*

Complete contact information is available at: https://pubs.acs.org/10.1021/acsomega.1c04275


### Notes

The authors declare no competing financial interest.

## ■ ACKNOWLEDGMENTS

This work was supported in part by the National Science Foundation (NSF DMR 1464111) and Linda and Bipin Doshi Endowment at the Missouri University of Science and Technology. The authors would like to thank Dr. Wei-Ting Chen at the Materials Research Center at the Missouri University of Science and Technology for SEM analysis.

## ■ REFERENCES

(1) Eskridge, D.; Foster, D.; Haight, D.; Kriese, L. Surgical apparatus and tools for same. US 20,060,217,729A1 2006.

(2) Bodenes, L.; Naturel, R.; Martinez, H.; Dedryvère, R.; Menetrier, M.; Croguennec, L.; Pérès, J.-P.; Tessier, C.; Fischer, F. Lithium secondary batteries working at very high temperature: Capacity fade and understanding of aging mechanisms. *J. Power Sources* **2013**, *236*, 265−275.

(3) Campion, C. L.; Li, W.; Lucht, B. L. Thermal decomposition of $LiPF_6$-based electrolytes for lithium-ion batteries. *J. Electrochem. Soc.* **2005**, *152*, A2327.
(4) Xu, K. Electrolytes and interphases in Li-ion batteries and beyond. *Chem. Rev.* **2014**, *114*, 11503−11618.
(5) Wang, Q.; Sun, J.; Yao, X.; Chen, C. Thermal behavior of lithiated graphite with electrolyte in lithium-ion batteries. *J. Electrochem. Soc.* **2006**, *153*, A329.
(6) Geng, Z.; Lu, J.; Li, Q.; Qiu, J.; Wang, Y.; Peng, J.; Huang, J.; Li, W.; Yu, X.; Li, H. Lithium metal batteries capable of stable operation at elevated temperature. *Energy Storage Mater.* **2019**, *23*, 646−652.
(7) Wu, T.; Chen, H.; Wang, Q.; Sun, J. Comparison analysis on the thermal runaway of lithium-ion battery under two heating modes. *J. Hazard. Mater.* **2018**, *344*, 733−741.
(8) Mosa, J.; Vélez, J. F.; Aparicio, M. Blend hybrid solid electrolytes based on LiTFSI doped silica-polyethylene oxide for lithium-ion batteries. *Membranes* **2019**, *9*, 109.
(9) Kato, Y.; Hori, S.; Saito, T.; Suzuki, K.; Hirayama, M.; Mitsui, A.; Yonemura, M.; Iba, H.; Kanno, R. High-power all-solid-state batteries using sulfide superionic conductors. *Nat. Energy* **2016**, *1*, 16030.
(10) Han, F.; Westover, A. S.; Yue, J.; Fan, X.; Wang, F.; Chi, M.; Leonard, D. N.; Dudney, N. J.; Wang, H.; Wang, C. High electronic conductivity as the origin of lithium dendrite formation within solid electrolytes. *Nat. Energy* **2019**, *4*, 187−196.
(11) Tian, H.-K.; Xu, B.; Qi, Y. Computational study of lithium nucleation tendency in $Li_7La_3Zr_2O_{12}$ (LLZO) and rational design of interlayer materials to prevent lithium dendrites. *J. Power Sources* **2018**, *392*, 79−86.
(12) Fenton, D. Complexes of alkali metal ions with poly (ethylene oxide). *Polymer* **1973**, *14*, 589.
(13) Croce, F.; Sacchetti, S.; Scrosati, B. Advanced, lithium batteries based on high-performance composite polymer electrolytes. *J. Power Sources* **2006**, *162*, 685−689.
(14) Abraham, K. M.; Alamgir, M. $Li^+$-conductive solid polymer electrolytes with liquid-like conductivity. *J. Electrochem. Soc.* **1990**, *137*, 1657.
(15) Zhou, W.; Wang, Z.; Pu, Y.; Li, Y.; Xin, S.; Li, X.; Chen, J.; Goodenough, J. B. Double-layer polymer electrolyte for high-voltage all-solid-state rechargeable batteries. *Adv. Mater.* **2019**, *31*, 1805574.
(16) Yue, L.; Ma, J.; Zhang, J.; Zhao, J.; Dong, S.; Liu, Z.; Cui, G.; Chen, L. All solid-state polymer electrolytes for high-performance lithium ion batteries. *Energy Storage Mater.* **2016**, *5*, 139−164.
(17) Fergus, J. W. Ceramic and polymeric solid electrolytes for lithium-ion batteries. *J. Power Sources* **2010**, *195*, 4554−4569.
(18) Zheng, J.; Tang, M.; Hu, Y. Y. Lithium ion pathway within $Li_7La_3Zr_2O_{12}$-polyethylene oxide composite electrolytes. *Am. Ethnol.* **2016**, *128*, 12726−12730.
(19) Wan, J.; Xie, J.; Kong, X.; Liu, Z.; Liu, K.; Shi, F.; Pei, A.; Chen, H.; Chen, W.; Chen, J.; Zhang, X.; Zong, L.; Wang, J.; Chen, L. Q.; Qin, J.; Cui, Y. Ultrathin, flexible, solid polymer composite electrolyte enabled with aligned nanoporous host for lithium batteries. *Nat. Nanotechnol.* **2019**, *14*, 705−711.
(20) Wu, N.; Chien, P. H.; Qian, Y.; Li, Y.; Xu, H.; Grundish, N. S.; Xu, B.; Jin, H.; Hu, Y. Y.; Yu, G.; Goodenough, J. B. Enhanced surface interactions enable fast $Li^+$ conduction in oxide/polymer composite electrolyte. *Angew. Chem., Int. Ed.* **2020**, *59*, 4131−4137.
(21) Costa, C.; Ribelles, J. G.; Lanceros-Méndez, S.; Appetecchi, G. B.; Scrosati, B. Poly (vinylidene fluoride)-based, co-polymer separator electrolyte membranes for lithium-ion battery systems. *J. Power Sources* **2014**, *245*, 779−786.
(22) Miao, R.; Liu, B.; Zhu, Z.; Liu, Y.; Li, J.; Wang, X.; Li, Q. PVDF-HFP-based porous polymer electrolyte membranes for lithium-ion batteries. *J. Power Sources* **2008**, *184*, 420−426.
(23) Chen, G.; Zhang, F.; Zhou, Z.; Li, J.; Tang, Y. A flexible dual-ion battery based on PVDF-HFP-modified gel polymer electrolyte with excellent cycling performance and superior rate capability. *Adv. Energy Mater.* **2018**, *8*, 1801219.
(24) Yang, X.; Zhang, F.; Zhang, L.; Zhang, T.; Huang, Y.; Chen, Y. A high-performance graphene oxide-doped ion gel as gel polymer electrolyte for all-solid-state supercapacitor applications. *Adv. Funct. Mater.* **2013**, *23*, 3353−3360.
(25) Xi, J.; Qiu, X.; Li, J.; Tang, X.; Zhu, W.; Chen, L. PVDF−PEO blends based microporous polymer electrolyte: Effect of PEO on pore configurations and ionic conductivity. *J. Power Sources* **2006**, *157*, 501−506.
(26) Wang, F.; Li, L.; Yang, X.; You, J.; Xu, Y.; Wang, H.; Ma, Y.; Gao, G. Influence of additives in a PVDF-based solid polymer electrolyte on conductivity and Li-ion battery performance. *Sustainable Energy Fuels* **2018**, *2*, 492−498.
(27) Wang, X.; Hao, X.; Cai, D.; Zhang, S.; Xia, X.; Tu, J. An ultraviolet polymerized 3D gel polymer electrolyte based on multi-walled carbon nanotubes doped double polymer matrices for lithium-sulfur batteries. *Chem. Eng. J.* **2020**, *382*, 122714.
(28) Bi, S.; Sun, C. N.; Zawodzinski, T. A., Jr.; Ren, F.; Keum, J. K.; Ahn, S. K.; Li, D.; Chen, J. Reciprocated suppression of polymer crystallization toward improved solid polymer electrolytes: Higher ion conductivity and tunable mechanical properties. *J. Polym. Sci., Part B: Polym. Phys.* **2015**, *53*, 1450−1457.
(29) Gupta, H.; Balo, L.; Singh, V. K.; Chaurasia, S. K.; Singh, R. K. Effect of phosphonium based ionic liquid on structural, electrochemical and thermal behaviour of polymer poly (ethylene oxide) containing salt lithium bis (trifluoromethylsulfonyl) imide. *RSC Adv.* **2016**, *6*, 87878−87887.
(30) Ramesh, S.; Lu, S.-C. Effect of nanosized silica in poly (methyl methacrylate)−lithium bis (trifluoromethanesulfonyl) imide based polymer electrolytes. *J. Power Sources* **2008**, *185*, 1439−1443.
(31) Sim, L. N.; Majid, S. R.; Arof, A. K. FTIR studies of PEMA/PVdF-HFP blend polymer electrolyte system incorporated with $LiCF_3SO_3$ salt. *Vib. Spectrosc.* **2012**, *58*, 57−66.
(32) Ramesh, S.; Liew, C.-W. Dielectric and FTIR studies on blending of [xPMMA−(1−x)PVC] with LiTFSI. *Measurement* **2013**, *46*, 1650−1656.
(33) Prabakaran, P.; Manimuthu, R. P. Enhancement of the electrochemical properties with the effect of alkali metal systems on PEO/PVdF-HFP complex polymer electrolytes. *Ionics* **2016**, *22*, 827−839.
(34) Elashmawi, I. S.; Gaabour, L. H. Raman, morphology and electrical behavior of nanocomposites based on PEO/PVDF with multi-walled carbon nanotubes. *Results Phys.* **2015**, *5*, 105−110.
(35) Vignarooban, K.; Dissanayake, M. A. L. K.; Albinsson, I.; Mellander, B.-E. Effect of $TiO_2$ nano-filler and EC plasticizer on electrical and thermal properties of poly (ethylene oxide)(PEO) based solid polymer electrolytes. *Solid State Ionics* **2014**, *266*, 25−28.
(36) Kumar, B.; Scanlon, L. G. Polymer-ceramic composite electrolytes. *J. Power Sources* **1994**, *52*, 261−268.
(37) Zhang, J.; Zhao, N.; Zhang, M.; Li, Y.; Chu, P. K.; Guo, X.; Di, Z.; Wang, X.; Li, H. Flexible and ion-conducting membrane electrolytes for solid-state lithium batteries: Dispersion of garnet nanoparticles in insulating polyethylene oxide. *Nano Energy* **2016**, *28*, 447−454.
(38) Wen, J.; Zhang, R.; Zhao, Q.; Liu, W.; Lu, G.; Hu, X.; Sun, J.; Wang, R.; Jiang, X.; Hu, N.; Liu, J.; Liu, X.; Xu, C. Hydroxyapatite nanowire-reinforced poly (ethylene oxide)-based polymer solid electrolyte for application in high-temperature lithium batteries. *ACS Appl. Mater. Interfaces* **2020**, *12*, 54637−54643.
(39) Wen, J.; Zhao, Q.; Jiang, X.; Ji, G.; Wang, R.; Lu, G.; Long, J.; Hu, N.; Xu, C. Graphene oxide enabled flexible PEO-based solid polymer electrolyte for all-solid-state lithium metal battery. *ACS Appl. Energy Mater.* **2021**, *4*, 3660−3669.
(40) Ein-Eli, Y.; Markovsky, B.; Aurbach, D.; Carmeli, Y.; Yamin, H.; Luski, S. The dependence of the performance of Li-C intercalation anodes for Li-ion secondary batteries on the electrolyte solution composition. *Electrochim. Acta* **1994**, *39*, 2559−2569.
(41) Verma, P.; Maire, P.; Novák, P. A review of the features and analyses of the solid electrolyte interphase in Li-ion batteries. *Electrochim. Acta* **2010**, *55*, 6332−6341.
(42) Aurbach, D.; Markovsky, B.; Shechter, A.; Ein-Eli, Y.; Cohen, H. A comparative study of synthetic graphite and Li electrodes in


https://doi.org/10.1021/acsomega.1c04275
*ACS Omega* 2021, 6, 29060−29070

electrolyte solutions based on ethylene carbonate-dimethyl carbonate mixtures. *J. Electrochem. Soc.* **1996**, *143*, 3809.
(43) Steiger, J.; Richter, G.; Wenk, M.; Kramer, D.; Mönig, R. Comparison of the growth of lithium filaments and dendrites under different conditions. *Electrochem. Commun.* **2015**, *50*, 11−14.
(44) Evans, J.; Vincent, C. A.; Bruce, P. G. Electrochemical measurement of transference numbers in polymer electrolytes. *Polymer* **1987**, *28*, 2324−2328.



https://doi.org/10.1021/acsomega.1c04275
*ACS Omega* 2021, 6, 29060−29070